Pergamon

Int. J. Heat Mass Transfer. Vol. 37, Suppl. 1, pp. 149–160, 1994
Copyright © 1994 Elsevier Science Ltd
Printed in Great Britain. All rights reserved
0017–9310/94 $6.00 + 0.00

0017–9310(93)E0058–O

Convective mass transfer and pressure loss characteristics of staggered short pin-fin arrays

R. J. GOLDSTEIN, M. Y. JABBARI and S. B. CHEN

Heat Transfer Laboratory, Department of Mechanical Engineering, University of Minnesota, Minneapolis, MN 55455, U.S.A.

Abstract—The effect of fin shape on the mass transfer and pressure loss of a ten-row staggered short pin-fin array in fully developed approaching flow is investigated experimentally using three different fin shapes. The Reynolds number, based on approach-velocity and fin diameter, ranges from 3000 to 18 000. The fin shape affects the row-by-row variation of Sherwood number. The results indicate that the stepped-diameter circular fin arrays have not only a larger mass transfer coefficient, but also a smaller pressure loss compared to a uniform-diameter circular fin array. In stepped-diameter circular fin arrays, the effect of step-length-to-total-length ratio on Sherwood number is small, but the total mass transfer rate and pressure loss change significantly with this ratio, owing to differences in mass transfer area and free flow area, respectively.

1. INTRODUCTION

EXTENSIVE research for short pin-fin arrays to augment convective heat transfer in a rectangular duct with large aspect ratio has been performed since the early 1980s, to provide information needed for designing more effective internal cooling in the after-region of a turbine blade, as well as the cooling of circuit boards in electronic equipment. The effects of length-to-diameter ratio of fin, array geometry, entrance length, and fin shape on heat transfer and pressure loss have been investigated. Heat transfer and pressure loss in the presence of lateral flow ejection, channel convergence, array interruption, and the change of array configuration also have been studied to simulate specific operating conditions for the internal cooling of a turbine blade. The research in this area up to 1987 is well reviewed by Armstrong and Winstanley [1].

The results of these studies show that short pin-fin arrays produce higher heat transfer than plain channels without pin fins. However, the increase in heat transfer is always accompanied by a substantial increase in pressure loss. In most applications of pin fins, both the heat transfer and the pressure loss characteristics must be considered. In cooling a turbine blade, for example, minimum cooling air flow and minimum pressure loss are desired, because the cooling air is supplied by the compressor at the cost of turbine cycle performance. To improve the heat transfer and pressure loss characteristics of the short pin-fin array, better understanding of the physical mechanisms which govern both the heat transfer and the pressure loss is essential. Owing to the small length-to-diameter ratio, much of the heat transfer area of the short pin-fin channel is affected by the strong endwall–cylinder interaction (endwall effect).

Several reports show high mass transfer in a developing boundary layer near the base of a protruding cylinder; Goldstein and Karni [2], Karni and Goldstein [3], Van Dresar and Mayle [4], and Goldstein *et al.* [5]. The horseshoe vortex system generated at the cylinder–endwall junction plays an important role in heat transfer augmentation on both the cylinder and the endwall. Augmentation of heat transfer by placing a cylinder in a fully developed duct flow is reported by Ireland and Jones [6]. They found that a horseshoe vortex system was also generated near the fin–endwall junction in a fully developed duct flow, and this induced an augmentation of heat transfer from the duct wall in the vicinity of the cylinder.

Mass transfer and flow characteristics on the endwall behind a short protruding cylinder with a free end are reported by Goldstein *et al.* [7], and Kawamura *et al.* [8, 9]. They observed that the fluid flowing over the free end of a short protruding cylinder is dragged into the wake and touches down on the endwall. As a result, the cylinder with a free end results in higher endwall mass transfer than a long cylinder, and the magnitude of this increase depends on the boundary layer thickness and the length of the cylinder. Chyu and Goldstein [10] also report that the endwall mass transfer of an array of short cylinders with free end ($H/d = 1$) is remarkably higher than that of an array of long cylinders.

Based on these results, a new fin shape, which has potential to improve the heat/mass transfer and pressure loss characteristics, is considered. The new fin is a stepped-diameter circular fin composed of three coaxial circular cylinders with stepwise change of diameter. The cylinders at both ends have equal diameters and the one in the middle has a reduced diameter. With this fin shape, the flow going over the step of the cylinder may be dragged into the wake, wash the side of larger cylinder and touch down on the endwall behind the cylinder. Owing to the interaction of the vortices shed from the larger and smaller cylinders, the turbulence level of the wake may be increased. Moreover, with this shape, the heat transfer area on the fin and free flow area can be increased. These effects of the stepped-diameter circular fin may work

NOMENCLATURE

a_0, a_1, a_2 coefficients of equations (12), (13), and (16)
b_0, b_1, b_2 exponents of equations (12), (13), and (16)
A_{duct} cross-sectional area of the duct (Table 1)
A_{min} minimum free flow area of the pin-fin channel (Table 1)
A_w mass transfer area on a fin surface (Table 1)
d fin diameter or fin major diameter (Fig. 2 and Table 1)
d_m diameter of the middle cylinder of SDCF1 and SDCF2 (Fig. 2 and Table 1)
D_h hydraulic diameter of unobstructed duct (= 44.45 mm in present study)
D_{na} binary diffusion coefficient of naphthalene in air (equation (3))
f friction factor (equation (9))
f^* modified friction factor (equation (10))
h_m mass transfer coefficient on the fin (equation (1))
H height of duct and length of fin (Fig. 2 and Table 1)
H_m length of the middle cylinder of SDCF1 and SDCF2 (Fig. 2 and Table 1)
H_s length of the cylinders at both ends of SDCF1 and SDCF2 (Fig. 2 and Table 1)
P static pressure
P_{atm} atmospheric pressure
Pr Prandtl number of air ($Pr = 0.71$)
$Re_{d,ave}$ Reynolds number based on characteristic velocity V_{ave} (equation (7))
$Re_{d,max}$ Reynolds number based on characteristic velocity V_{max} (equation (6))
s_x streamwise pitch of the pin-fin array (Fig. 2)
s_y spanwise pitch of the pin-fin array (Fig. 2)
Sc Schmidt number, ν/D_{na} ($Sc = 2.28$ at 25°C)
Sh_d Sherwood number of fin (equation (2))
$Sh_{d,f}$ fully developed Sherwood number (equation (4))
$(Sh_d)_i$ Sherwood number of fin in row i
$\overline{Sh}_d$ array-averaged Sherwood number (equation (5))
SDCF stepped-diameter circular fins, SDCF1 and SDCF2
SDCF1 stepped-diameter circular fin with $d_m/d = 0.7$ and $H_s/H = 1/3$ (Fig. 2)
SDCF2 stepped-diameter circular fin with $d_m/d = 0.7$ and $H_s/H = 1/4$ (Fig. 2)
UDCF uniform-diameter circular fin (Fig. 2)
T_w temperature at the fin surface [K]
V_{ave} mean velocity in unobstructed duct or mean approach-velocity
V_{max} maximum velocity at the minimum free flow area
x streamwise coordinate ($x = 0$ at the inlet baffle plate)
W width of rectangular duct.

Greek symbols
δm net mass of subliminated naphthalene (about 90 mg)
ΔP_{test} pressure drop across the test section
δt running time
μ dynamic viscosity of air
ν kinematic viscosity of air, μ/ρ
ρ density of air
$\rho_{n,a}$ naphthalene vapor density in free stream
$\rho_{n,w}$ naphthalene vapor density on fin surface.

to increase the heat transfer rate and decrease pressure loss compared to the uniform-diameter circular fin. The objective of this research is to verify this conjecture experimentally.

2. EXPERIMENTAL APPARATUS AND PROCEDURES

Mass transfer using naphthalene ($C_{10}H_8$) sublimination is used in this study. This technique has several advantages over a direct heat transfer experiment. Accurate measurement of transport coefficients is possible using this technique, which is extremely difficult in a heat transfer experiment, owing to conduction error. The boundary condition in mass transfer experiments is equivalent to an isothermal wall temperature condition in heat tarnsfer which is difficult to realize. This condition is especially beneficial in the study of fin heat transfer, because it corresponds to the condition that the efficiency of the fins is equal to one. In the present study only one fin in a designated location is naphthalene active, and the other fins and the endwalls do not participate in the mass transfer. This corresponds to the local thermal simulation methods frequently used in heat transfer experiments for an array of cylinders.

A schematic of the open-circuit suction-type wind tunnel used is presented in Fig. 1. The tunnel is composed of a rectangular duct, plenum chamber, orifice metering section, flow control valve, blower, and

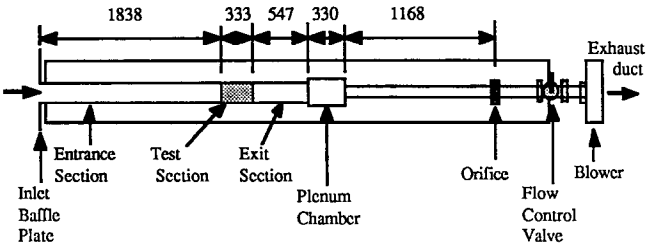

FIG. 1. Schematic view of wind tunnel (dimensions in mm).

exhaust duct. The rectangular duct made of aluminum plates has inner cross-sectional dimensions of 133.35 mm × 26.67 mm ($D_h = 44.5$), duct aspect ratio (W/H) of 5 to 1, and a total length of 2718 mm ($61.1D_h$). The initial portion of the rectangular duct, the entrance section, with length of 1837.5 mm ($41.3D_h$), serves as the hydrodynamically developing region. The last portion of the rectangular duct, the exit section, with length of 546.9 mm ($12.3D_h$), serves as the hydrodynamically redeveloping region. The test section with length of 333.3 mm ($7.5D_h$) is located between these two and contains the pin-fin array. A thin plate, sharp-edged orifice meter is used to measure air flow rate. Laboratory air is drawn into the duct and vented out of the laboratory after the blower.

Figure 2 presents the fin shapes and the array configuration. Three fin shapes are used. One is a uniform-diameter circular fin (denoted by UDCF). The other two are stepped-diameter circular fins (denoted by SDCF). All fins have the same diameter at both ends ($d = 13.34$ mm) and total length ($H = 26.67$ mm), with the resulting length-to-diameter ratio (H/d) of 2. Both stepped fins have the same reduced diameter in the middle ($d_m = 9.40$ mm) and, accordingly, a diameter reduction ratio (d_m/d) of 0.7. The difference between the two stepped fins is in the location of the steps in the direction of the fin axis. One has a step-length-to-total-length ratio (H_s/H) of 1/3 (denoted by SDCF1), and the other has H_s/H of 1/4 (denoted by SDCF2). The fins are arranged in a staggered manner with the same streamwise and spanwise pitch-to-diameter ratios (s_x/d and s_y/d) of 2.5. The number of rows in the streamwise direction is ten. Dimensions of the fins and arrays are presented in Table 1.

All fins intended to hold naphthalene are undercut by about 0.38 mm and fine threads are machined on the undercut surface to secure firm attachment of the

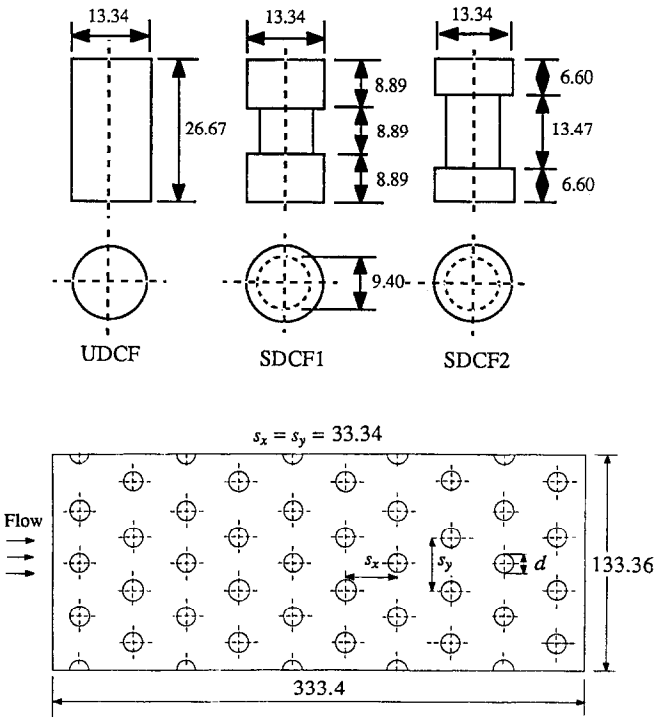

FIG. 2. Fin shapes and array configuration (dimensions in mm).

Table 1. Dimensions of fins and arrays

	Fins						Arrays			
Name	d (mm)	d_m (mm)	H (mm)	H_s (mm)	H_m (mm)	A_w (cm^2)	s_x/d	s_y/d	A_{duct} (cm^2)	A_{min} (cm^2)
UDCF	13.34	—	26.67	—	—	11.17	2.5	2.5	35.56	21.34
SDCF1	13.34	9.40	26.67	8.89	8.89	11.47	2.5	2.5	35.56	22.74
SDCF2	13.34	9.40	26.67	6.60	13.47	10.91	2.5	2.5	35.56	23.46

naphthalene. The coating of naphthalene on the fin is done by dipping the undercut fin into molten naphthalene. Best results are obtained when the temperature of the molten naphthalene is just below the boiling temperature (217.99°C). The naphthalene-coated fins are precisely machined (± 0.001 in. tolerance) using special tools and a holding device. They have excellent finished surfaces with sharp edges and corners. A group of naphthalene-coated fins are prepared at a time for successive data runs. After machining, the fins are put into separate plastic wraps and placed in a sealed plastic box to minimize excess sublimation loss by natural convection. The plastic box is stored in a laboratory for at least 8 h before a run to ensure thermal equilibrium with the laboratory environment. In each run, as mentioned above, only one naphthalene-coated fin is used. In successive runs of the same Reynolds number and same fin shape, only the streamwise location of the naphthalene-coated fin is changed, i.e. from the first row to the second row, etc. The coated fin is positioned as close as possible to the spanwise center of the duct to eliminate possible sidewall effects. Before and after a run, the coated fin is weighed using a Satorius 2432 balance which has a maximum scale capacity of 200 g and a resolution of 0.1 mg.

Twenty-seven pressure taps drilled on the top wall along the streamwise direction are used to measure the static pressure distribution along the rectangular duct. The signals sensed by a pressure transducer (Setra 239) are transmitted to a HP-85 microcomputer via a multimeter (Fluke 8840-A) and are time-averaged.

3. DATA REDUCTION

The mass transfer coefficient of a fin is determined from

$$h_m = \frac{\delta m}{(\rho_{n,w} - \rho_{n,a}) A_w \delta t}, \tag{1}$$

where δm is the measured change in mass of the naphthalene-coated fin, δt is the duration of run, A_w is the mass transfer area on the fin, and $(\rho_{n,w} - \rho_{n,a})$ is a difference in naphthalene vapor density between the surface of the fin and the approaching air. The naphthalene vapor density in the approach flow, $\rho_{n,a}$, is zero in the present study. The naphthalene vapor density on the fin, $\rho_{n,w}$, is calculated from the vapor pressure–temperature relation of naphthalene by Ambrose *et al.* [11] in conjunction with the ideal gas law.

The final result is expressed in terms of the Sherwood number. The Sherwood number for a given fin is defined by

$$Sh_d = \frac{h_m d}{D_{na}}, \tag{2}$$

where d is the diameter of fin and D_{na} is the binary diffusion coefficient of naphthalene in air. Values of D_{na} measured by many investigators show large discrepancies. Based on the detailed discussion in Chen [12], D_{na} is calculated from

$$D_{na} = D_{na,298}\left(\frac{T_w}{298.16}\right)^{1.93}\left(\frac{0.1013}{P}\right), \tag{3}$$

where $D_{na,298}$ ($= 0.0681$ cm^2 s^{-1}) is the diffusion coefficient at 298 K and 0.1013 MPa, and P is the pressure in MPa.

The fully developed Sherwood number and the array-averaged Sherwood number are also used. When the Sherwood number remains approximately constant for rows downstream of the nth row, the fully developed Sherwood number is calculated from

$$Sh_{d,f} = \frac{1}{10-n}\sum_{i=n+1}^{10}(Sh_d)_i \tag{4}$$

and the array-averaged Sherwood number is calculated from

$$\overline{Sh_d} = \frac{1}{10}\sum_{i=1}^{10}(Sh_d)_i. \tag{5}$$

Using the method of Kline and Mcklintock [13], the experimental uncertainty of Sherwood number in this experiment is estimated to be 5.4%.

Two types of Reynolds numbers are used to characterize the flow condition. One is a Reynolds number based on the maximum velocity (V_{max}) at the minimum free flow area (A_{min}) and fin diameter (d),

$$Re_{d,max} = \frac{\rho V_{max} d}{\mu}. \tag{6}$$

Another Reynolds number is based on the mean flow velocity (V_{ave}) in the unobstructed duct and the fin diameter (d),

$$Re_{d,ave} = \frac{\rho V_{ave} d}{\mu}. \quad (7)$$

Note that these two Reynolds numbers are related by

$$Re_{d,ave} = Re_{d,max}\left(\frac{A_{min}}{A_{duct}}\right), \quad (8)$$

where A_{duct} is a cross-sectional area of rectangular duct. The value of A_{min} depends on the shapes of fins. The A_{min}/A_{duct} values of the UDCF, SDCF1 and SDCF2 arrays are 0.60, 0.64 and 0.66, respectively.

Figure 3 represents a typical static pressure distribution along the duct which includes entrance section, test section, and exit section. The measured pressure data cannot be used directly to evaluate pressure loss across the pin-fin channel, owing to the entrance and exit effects. Therefore, the static pressures at one-half of the streamwise pitch ($s_x/2$) upstream from the first row and downstream from the last row are estimated by extrapolating the measured static pressure data. The difference of these two is the actual pressure loss across the pin-fin channel, and is denoted as ΔP_{test}. For the dimensionless presentation of the pressure loss across the pin–fin channel, ΔP_{test} is normalized by the number of rows, N, and the dynamic pressure, $(1/2)\rho V_{max}^2$

$$f = \frac{\Delta P_{test}}{\frac{1}{2}\rho V_{max}^2 N}. \quad (9)$$

Although this friction factor has been widely used in the previous studies of tube banks, it does not allow easy comparison of the results, because the values of V_{max} (and A_{min}) of the UDCF, SDCF1 and SDCF2 arrays are different even for the same flow rate. Therefore, a modified friction factor, based on the average flow velocity at the unobstructed duct, V_{ave},

$$f^* = \frac{\Delta P_{test}}{\frac{1}{2}\rho V_{ave}^2 N} \quad (10)$$

is also used. The relationship between f and f^* is given by

$$f^* = f\left(\frac{V_{max}}{V_{ave}}\right)^2 = f\left(\frac{A_{duct}}{A_{min}}\right)^2. \quad (11)$$

The $(A_{duct}/A_{min})^2$ values of the UDCF, SDCF1 and SDCF2 arrays are 2.78, 2.45 and 2.30, respectively.

4. RESULTS AND DISCUSSION

4.1. *Mass transfer*

Row-by-row variations of Sherwood number are presented in Figs. 4, 5, and 6 for the UDCF, SDCF1 and SDCF2 arrays, respectively. In each figure, six sets of Sherwood number, each corresponding to a specific Reynolds number, are plotted as a function of streamwise row number. Inspection of these figures reveals that the Sherwood number varies row-by-row in the initial rows and then reaches a constant 'fully developed' value that is independent of the row number in the array. The flow across the fin surface is expected to be complex, owing to the combined effects of the flow acceleration between the space of adjacent fins, vortex shedding behind the fins, and impingement of the vortices and accelerated flow from upstream rows on the front surface of the fins. Moreover, owing to the small length-to-diameter ratio, a large portion of the fin surface is affected by the complex endwall flow. Fins in the first row are influenced by the endwalls and the flow acceleration caused by the blockage of flow, both of which are common in all rows. Fins in the second row are additionally affected by the impingement of the accelerated flow. Fins in the third row experience additional effects of the impingement of the accelerated flow and the shed vortices. Fins in the subsequent rows experience the same flow characteristics as those in the third row,

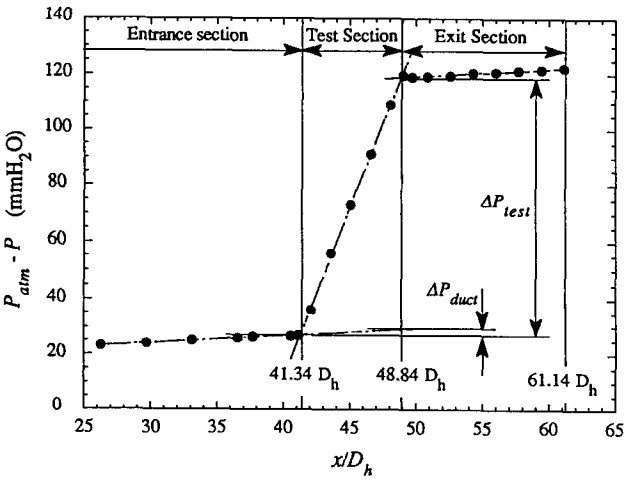

FIG. 3. Typical streamwise static pressure distribution in pin-fin channel (SDCF1 array, $Re_{d,max} = 17\,800$).

and this repeated flow condition shows in the fully developed mass transfer.

As expected, the Sherwood number increases as the Reynolds number increases. The developing patterns of the Sherwood number at the entrance regime are influenced by the fin shape and Reynolds number. For the UDCF array the Sherwood number, presented in Fig. 4, increases monotonically with row number in the initial rows and reaches its fully developed value at low Reynolds number, i.e. $Re_{d,max} = 5000$ and 10000. At higher Reynolds number, $Re_{d,max} \geqslant 15000$, the Sherwood number increases to the third row and then decreases slightly before reaching its fully developed value. As a result, a local peak of Sherwood number is evident at the third row where the vortices shed from the first row directly impinge on the fin. Even though a slight variation of Sherwood number can be noticed between the fourth row and the sixth row, this variation is less than the uncertainty in the experiment. Thus, from a practical point of view, it may be said that fully developed mass transfer condition of the UDCF array is established from the fourth row on.

The SDCF arrays show a different variation of Sherwood number. For the SDCF1 array, as can be observed in Fig. 5, the increase of Sherwood number at the initial three rows is similar to that for the UDCF array, but the decrease of Sherwood number in the fourth and the fifth rows, which is evident in the UDCF array at higher Reynolds number, is very mild—less than the uncertainty in the measurement. For the SDCF2 array, a decrease of Sherwood number is not observed in the fourth row (of Fig. 6); the Sherwood number continuously increases to the fourth row. Even though a mild decrease in Sherwood number is found in the fifth row, this decrease is less than the uncertainty in the experiment. Therefore, it may be said that the Sherwood number of the SDCF1 and SDCF2 arrays increases monotonically in the initial rows and reaches its fully developed value in the fourth row. The fully developed Sherwood numbers of the SDCF1 and SDCF2 arrays are higher than that of the UDCF array, apparently owing to the complex vortex flow generated by the steps.

A local peak of Sherwood number in an UDCF array was also observed by Metzger *et al.* [14], Simoneau and VanFossen [15], and Chyu [16], and the locations of the maximum Sherwood number in the present results correspond well with those of the maximum turbulence intensity measured by Metzger and Haley [17] and Simoneau and VanFossen [15]. However, the small but continuous decrease of the Sherwood number in the downstream rows following the peak, which was observed by Metzger *et al.* [14, 17] and Chyu [16], is not found in the present results, which may be due to the different mass/heat transfer boundary conditions in the different experiments.

It is important to compare present mass transfer results to existing heat transfer data. Comparison of the first row mass transfer results of the UDCF array to the corresponding heat transfer data is presented in Fig. 7. Plotted on the ordinate are Sherwood number scaled by $Sc^{0.4}$ and Nusselt number scaled by $Pr^{0.4}$. $Pr = 0.71$ is used and Sc is evaluated by $Sc = \nu/D_{na}$ ($= 2.28$ and 25°C), where ν is the kinematic viscosity of air in view of the minute naphthalene vapor concentration. In this figure the present mass transfer results ($H/d = 2$, $s_x/d = s_y/d = 2.5$) are compared to the heat transfer data by Simoneau and VanFossen [15] ($H/d = 3.01$, $s_x/d = s_y/d = 2.67$) and Metzger *et al.* [14] ($H/d = 1$, $s_x/d = s_y/d = 2.5$). In the experiment of Simoneau and VanFossen [15], as in the present experiment, only one fin in a desired location was active and the endwalls did not participate in the heat transfer, whereas, in the study of Metzger *et al.* [14], both the fins and endwalls participated in the heat transfer.

The present results show good agreement with

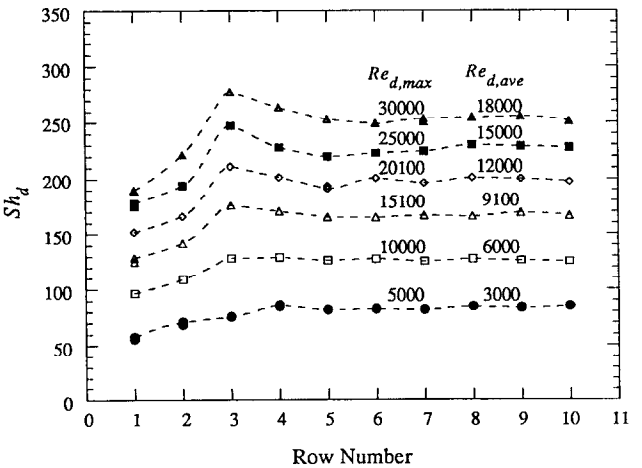

FIG. 4. Sherwood number of the UDCF array.

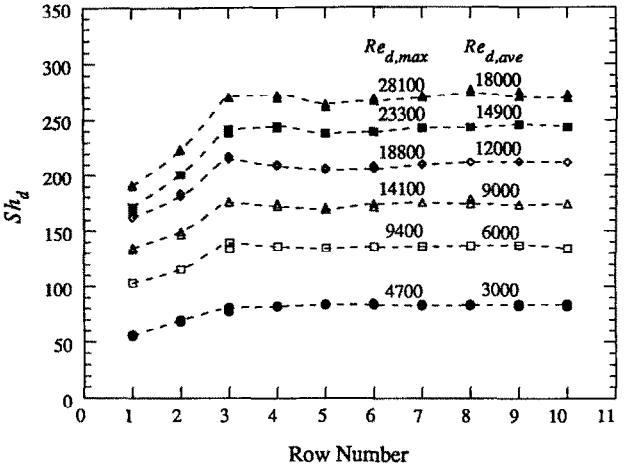

FIG. 5. Sherwood number of the SDCF1 array.

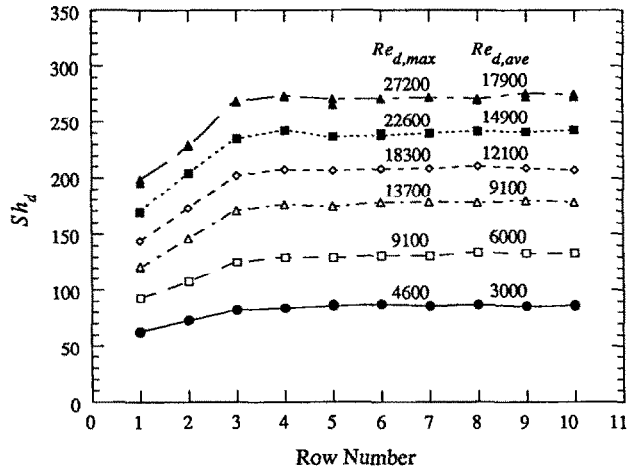

FIG. 6. Sherwood number of the SDCF2 array.

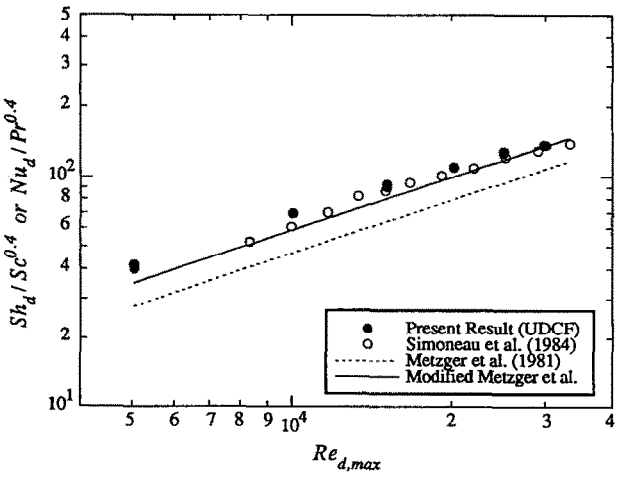

FIG. 7. Comparison of the first row Sherwood number of the UDCF arrays.

Simoneau and VanFossen [15], but a large deviation from Metzger *et al.* [14]. From a practical point of view, direct comparison with Metzger *et al.* [14] is not appropriate, since their data include the heat transfer from both the fin and the endwall. However, this comparison may provide some insight into the ratio of heat transfer coefficients between the fin and the endwall, which have shown diversity in previous studies. VanFossen [18] predicted that the heat transfer coefficient on the fin would be higher than that on the endwall by about 35%. Metzger and Haley [17] reported that the heat transfer coefficients on the fin and the endwall were comparable within $\pm 10\%$. Later, Metzger *et al.* [19] cautiously predicted that the heat transfer coefficient on the fin was two times higher than that on the endwall. Chyu [16] reported that the ratio of Sherwood numbers between the fin and the endwall were comparable within $\pm 10\%$ based on his mass transfer experiment. No direct comparison of the measured data was performed in those studies except by Chyu [16]. Even though more studies are needed to determine this relative value, the present results favor the prediction by VanFossen. The solid line in Fig. 7 represents the calculated first row heat transfer coefficients of the fin from the result of Metzger *et al.* [14], under the assumption that the heat transfer coefficient of the fin is higher than that of the endwall by 35%. This line shows relatively good agreement with the present results.

The variation with Reynolds number of the fully developed Sherwood number and the array-averaged Sherwood number, are represented in Figs. 8 and 9, respectively. Note that the array-averaged Sherwood numbers are lower than the corresponding fully developed values. Generally, the SDCF arrays show higher mass transfer coefficients than the UDCF array, and the level of this difference increases as the Reynolds number increases. One unexpected observation from these figures is that the array-averaged and the fully developed Sherwood numbers of the SDCF arrays are not influenced significantly by the location of step in the fin axial direction. The differences in the array-averaged and the fully developed Sherwood numbers between the SDCF1 and the SDCF2 arrays are very small. The relative increases of the array-averaged Sherwood number of the SDCF arrays over the UDCF array at the Reynolds number $Re_{d,max} = 10000$, 20000 and 30000 are 8.23, 9.74, 10.6% for SDCF1 array and 9.9, 10.8, 11.3% for SDCF2 array, respectively.

As can be seen from these figures, the array-averaged Sherwood number and fully developed Sherwood number are well correlated by the least-square curve fitting,

$$\overline{Sh_d} = a_0 Re_{d,max}^{b_0} \tag{12}$$

$$Sh_{d,f} = a_1 Re_{d,max}^{b_1}, \tag{13}$$

where the coefficients and exponents of the equations are given in Table 2. When the different geometric factors of the UDCF, SDCF1 and SDCF2 are included, as shown in Fig. 10, all the $\overline{Sh_d}$ and the $Sh_{d,f}$ data can be correlated by

$$\overline{Sh_d} = 0.299\, Re_{d,max}^{0.653}\left(\frac{2H_s}{H}\right)^{-0.044}\left(\frac{d_m}{d}\right)^{-0.193} \tag{14}$$

$$Sh_{d,f} = 0.327\, Re_{d,max}^{0.647}\left(\frac{2H_s}{H}\right)^{-0.068}\left(\frac{d_m}{d}\right)^{-0.194}, \tag{15}$$

where $2H_s/H = 1.0$, 0.6667 and 0.5, and $d_m/d = 1.0$, 0.7 and 0.7 for the UDCF, SDCF1 and SDCF2 arrays, respectively. Equations (14) and (15) give a convenient way to compare the relative mass transfer performance of the UDCF, SDCF1 and SDCF2 arrays. A summary of the performance comparison using these correlation equations is given in the Appendix.

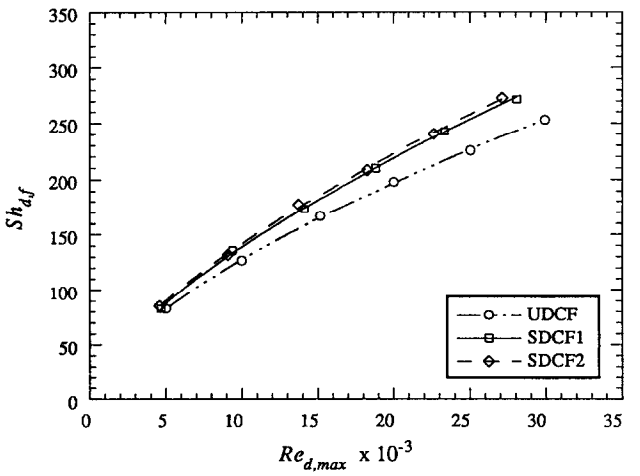

FIG. 8. Fully developed Sherwood number of the UDCF, SDCF1 and SDCF2 arrays.

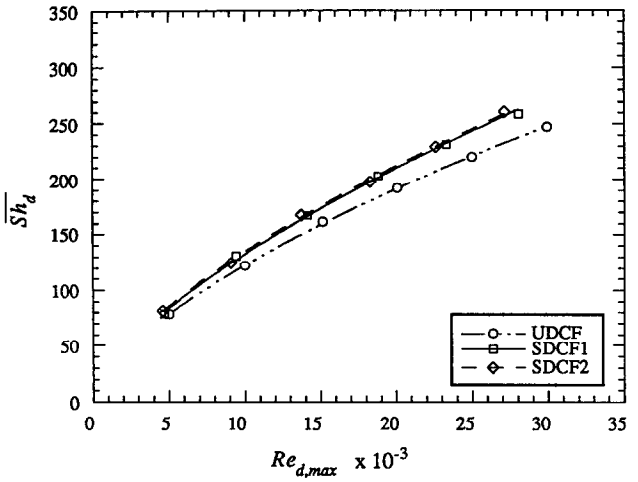

FIG. 9. Array-averaged Sherwood number of the UDCF, SDCF1 and SDCF2 arrays.

Table 2. The coefficients and exponents of equations (12) and (13)

	$\overline{Sh_d}$ (equation (12))		$Sh_{d,f}$ (equation (13))	
Arrays	a_0	b_0	a_1	b_1
UDCF	0.331	0.642	0.392	0.628
SDCF1	0.298	0.662	0.320	0.659
SDCF2	0.327	0.654	0.346	0.653

4.2. *Pressure loss*

The streamwise pressure distribution along the rectangular duct with and without fins is measured. The friction factors of the unobstructed duct show good agreement with the well-known friction factor correlations for fully developed flow by Blasius *et al.* taken from Kays and Crawford [20], and provide support for the fully developed flow assumption. The friction factors for the UDCF, SDCF1 and SDCF2 arrays are presented in Fig. 11. Comparison of the present results with the correlation equation suggested by Metzger *et al.* [21] for staggered arrays of uniform diameter fins ($H/d = 1$, $s_y/d = 2.5$, $s_x/d = 1.05 \sim 5.0$ and $N = 10$) is also made. The present results for the UDCF array show good agreement to the thick solid line, which corresponds to the correlation equation by Metzger *et al.* [21]. They reported that all of their results fell within $\pm 15\%$ of the correlation equation (two dashed lines). All the present results also lie in this range.

The friction factor has a different Reynolds number dependence at high Reynolds number than it does at low Reynolds number, as noticed by Metzger *et al.* [21]. The friction factors vary less for $Re_{d,max} < 11\,000$ than for $Re_{d,max} > 11\,000$. The friction factors are well represented by least-square curve fitting in the form of

$$f = a_2 Re_{d,max}^{b_2}, \tag{16}$$

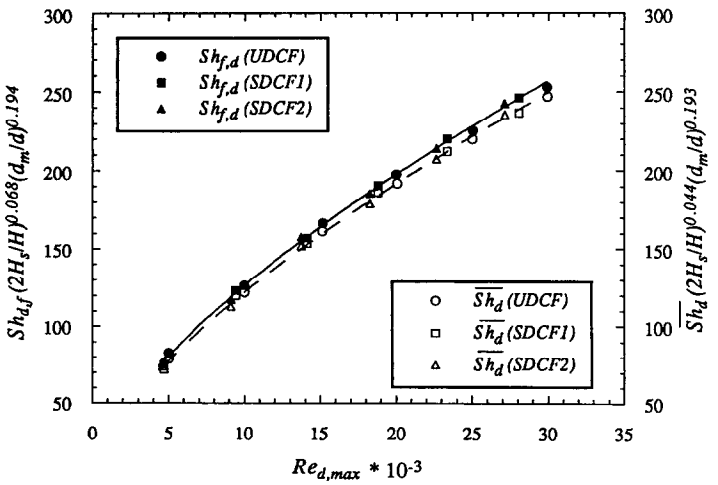

FIG. 10. General correlation for the array-averaged and fully developed Sherwood numbers.

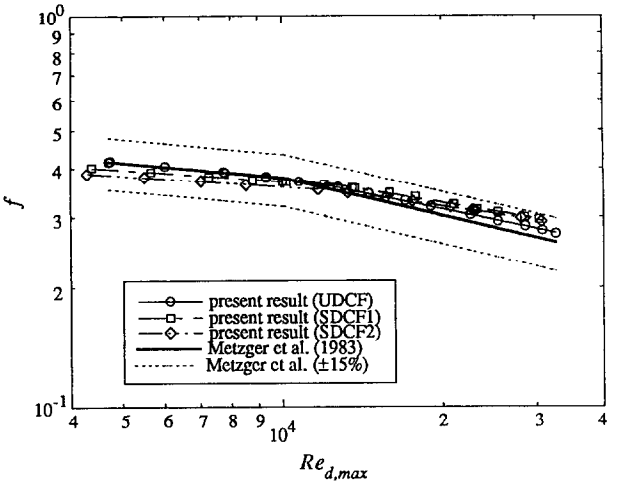

FIG. 11. Friction factors of the UDCF, SDCF1 and SDCF2 arrays.

Table 3. The coefficient and exponent of equation (16)

	$Re_{d,max} < 11\,000$		$Re_{d,max} > 11\,000$	
Arrays	a_2	b_2	a_2	b_2
UDCF	1.371	−0.141	5.018	−0.280
SDCF1	0.917	−0.099	3.160	−0.229
SDCF2	0.841	−0.093	2.240	−0.197

where the coefficient and exponent of the equation are presented in Table 3.

Comparisons of the pressure losses of the UDCF and SDCF arrays are obscure in this figure, since both the friction factor and the Reynolds number are defined based on the maximum flow velocity at the minimum free flow area, the values of which depend on the fin shape even at the same flow rate condition. Therefore, the modified friction factor, f^*, and Reynolds number based on the mean approach-flow velocity in the unobstructed duct, $Re_{d,ave}$, are thought to be appropriate for making comparisons.

The modified friction factors for the UDCF, SDCF1 and SDCF2 arrays are presented in Fig. 12. The friction factor for the UDCF array is noticeably higher than those for the SDCF1 and SDCF2 arrays, but the magnitudes of these differences diminish as the Reynolds number increases. It may be said that two factors play important roles in the pressure loss characteristics of the stepped-diameter circular fin arrays. One is a reduced blockage to the flow which decreases pressure loss. Another is a separation of flow induced by the step which increases pressure loss. The effect of a reduced blockage to the flow may be the dominant parameter at low Reynolds number. As the Reynolds number increases, the role of flow separation gradually increases and the pressure loss gradually approaches that for the UDCF array. Between the SDCF arrays, the SDCF1 array shows

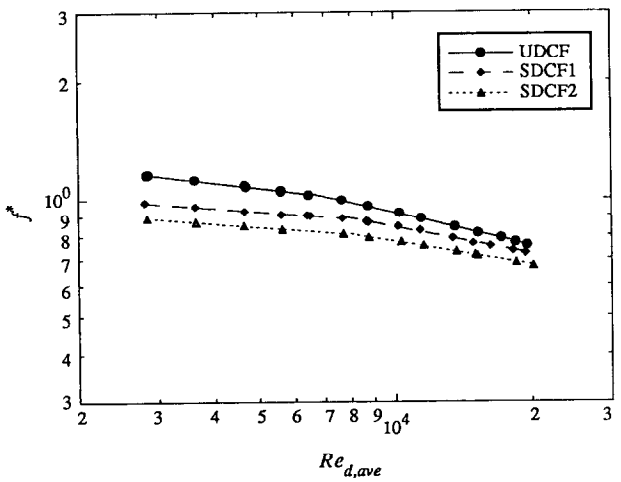

FIG. 12. Modified friction factors of the UDCF, SDCF1 and SDCF2 arrays.

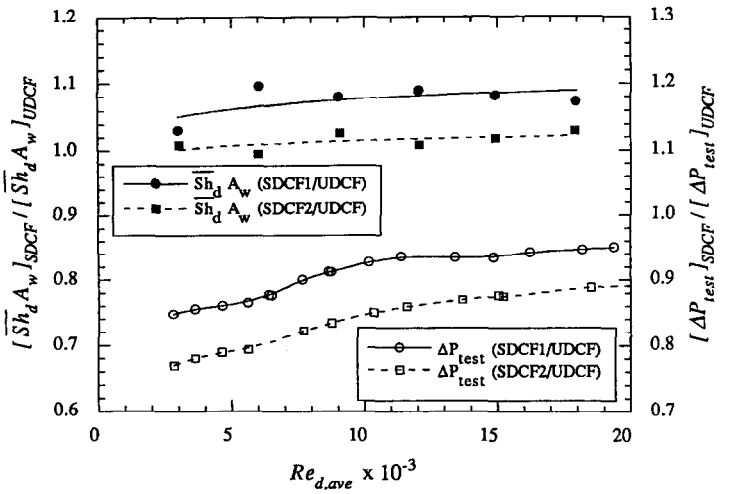

FIG. 13. Comparison of the mass transfer rate and the pressure loss of the UDCF, SDCF1 and SDCF2 arrays.

higher modified friction factors than the SDCF2 array.

4.3. *Overall performance*

To compare the overall peformance of the UDCF, SDCF1 and SDCF2 arrays, the differences in mass transfer area and free flow area have to be considered. Figure 13 represents a comparison of the mass transfer rate and pressure loss at the same mean approach-flow velocity (V_{ave}) condition. The ordinate of this figure has dual labels. One is a ratio of mass transfer rate between the SDCF and UDCF arrays, $(\overline{Sh}_d A_w)_{SDCF}/(\overline{Sh}_d A_w)_{UDCF}$. Another is a ratio of pressure loss between the SDCF and UDCF arrays, $(\Delta P_{test})_{SDCF}/(\Delta P_{test})_{UDCF}$.

It can be observed that the SDCF arrays yield better mass transfer rates than the UDCF array, and the level of this mass transfer enhancement increases as the Reynolds number increases. Between the SDCF arrays, the SDCF1 array shows better mass transfer performance than the SDCF2 array, mainly due to the difference in the mass transfer area $[(A_w)_{SDCF1}/(A_w)_{SDCF2} = 1.052]$. The increases of the mass transfer rate of the SDCF arrays relative to the UDCF array are, on average, 7.5% and 1.4% for the SDCF1 and SDCF2 array, respectively, for the range of Reynolds numbers tested.

This figure clearly shows that it is possible to reduce pressure loss of the conventional UDCF array using the SDCF array. The SDCF2 array shows better performance than the SDCF1 array in reducing pressure loss over the whole range of Reynolds numbers tested. The decreases of pressure loss of the SDCF arrays relative to the UDCF array at the Reynolds number $Re_{d,ave} = 3000$, 10000 and 18000 are 15%, 7% and 5% for the SDCF1 array, and 23%, 15% and 11% for the SDCF2 array, respectively.

5. SUMMARY AND CONCLUSION

In this study, naphthalene sublimation is employed to investigate the effects of fin shape on the mass transfer and pressure loss of staggered arrays of short pin fins. The Sherwood number varies in the initial rows, and then reaches a fully developed value from the fourth row on for all arrays tested. The developing patterns of the Sherwood number in the initial rows depend somewhat on the fin shape. In the UDCF array, the initial increase of the Sherwood number is followed by a slight decrease before a fully developed value is reached. In contrast, the Sherwood number essentially increases monotonically in the initial rows of the SDCF arrays, and then reaches the fully developed value without a local peak of Sherwood number.

The fully developed and the array-averaged Sherwood numbers are higher with the SDCF arrays than those of UDCF array. Between the SDCF arrays, no clear differences in the row-by-row variation patterns are observed. On average, the SDCF1 and SDCF2 arrays show 9% and 10% higher Sherwood numbers, and 12% and 8% higher mass transfer rates than the UDCF array, respectively, at the same channel characteristic velocity, V_{max}. At the same approach-flow velocity (V_{ave}) condition, on average, the SDCF1 and SDCF2 arrays show 5% and 4% higher Sherwood numbers and 8% and 1% higher mass transfer rate than the UDCF array, respectively. This difference in mass transfer rate between the SDCF1 and SDCF2 arrays is mainly due to the difference in mass transfer area.

The SDCF arrays cause less pressure loss than the UDCF array. Between the SDCF arrays, the SDCF2 array shows substantially lower pressure loss than the SDCF1 array, probably due to the reduced flow blockage. On average, the SDCF1 and SDCF2 arrays

show 9% and 16% less pressure loss than that of the UDCF array, respectively, at the same approach-flow condition.

REFERENCES

1. J. Amstrong and D. Winstanley, A review of staggered array pin fin heat transfer for turbine cooling applications, *ASME J. Turbomachinery* **110,** 94–103 (1988).
2. R. J. Goldstein and J. Karni, The effect of a wall boundary layer on local mass transfer from a cylinder in crossflow, *ASME J. Heat Transfer* **106,** 260–267 (1984).
3. J. Karni and R. J. Goldstein, Endwall effects on local mass transfer from a cylinder in crossflow, *Proc. 2nd Int. Symp. Refined Flow Modeling and Turbulence Measurement*, Vol. 1, pp. 1–33 (1985).
4. N. Van Dresar and R. E. Mayle, Convection at the base of a cylinder with a horseshoe vortex, *Proc. 8th Int. Heat Transfer Conf.*, Vol. 3, pp. 1121–1126 (1986).
5. R. J. Goldstein, J. Karni and Y. Zhu, Effect of boundary conditions on mass transfer near the base of a cylinder in crossflow, *ASME J. Heat Transfer* **112,** 501–504 (1990).
6. P. T. Ireland and T. V. Jones, Detailed measurement of heat transfer on and around a pedestal in fully developed passage flow, *Proc. 8th Int. Heat Transfer Conf.*, Vol. 3, pp. 975–980 (1986).
7. R. J. Goldstein, M. K. Chyu and R. C. Hain, Measurement of local mass transfer on a surface in the region of the base of a protruding cylinder with a computer controlled data acquisiton system, *Int. J. Heat Mass Transfer* **28,** 977–985 (1985).
8. T. Kawamura, M. Hiwada, I. Mabuchi and M. Kumada, Augmentation of turbulent heat transfer on a flat plate with a three-dimensional protuberance (first report), *Bull. JSME* **27,** 2787–2794 (1984).
9. T. Kawamura, M. Hiwada, I. Mabuchi and M. Kumada, Augmentation of turbulent heat transfer on a flat plate with a three-dimensional protuberance (second report), *Bull. JSME* **28,** 283–291 (1985).
10. M. K. Chyu and R. J. Goldstein, Influence of an array of wall-mounted cylinders on the mass transfer from a flat surface, *Int. J. Heat Mass Transfer* **34,** 2175–2186 (1991).
11. D. Ambrose, I. J. Lawenson and C. H. S. Sprake, The vapor pressure of naphthalene, *J. Chem. Thermodyn.* **7,** 1173–1176 (1975).
12. S. B. Chen, The effect of fin shapes on the mass transfer and pressure drop of the staggered aray of short pin fins, MSME Thesis, University of Minnesota, Minneapolis, Minnesota (1992).
13. S. J. Kline and F. A. Mcklintock, Describing uncertainties in single sample experiments, *Mech. Engng* **75,** 3–8 (1953).
14. D. E. Metzger, R. A. Berry and J. P. Bronson, Developing heat transfer in rectangular ducts with arrays of short pin fins, ASME Paper No. 81-WA/HT-6 (1981).
15. R. J. Simoneau and G. J. VanFossen, Effect of location in an array on heat transfer to a short cylinder in crossflow, *ASME J. Heat Transfer* **106,** 42–48 (1984).
16. M. K. Chyu, Heat transfer and pressure drop for short pin-fin arrays with fin-endwall fillet, ASME Paper No. 89-GT-99 (1989).
17. D. E. Metzger and S. W. Haley, Heat transfer experiment and flow visualization for arrays of short pin fins, ASME Paper No. 82-GT-138 (1982).
18. G. J. VanFossen, Heat-transfer coefficients for staggered arrays of short fins, *ASME J. Engng Power* **104,** 268–274 (1981).
19. D. E. Metzger, C. S. Fan and S. W. Haley, Effects of fin shape and array orientation on heat transfer and pressure loss in pin fin array, *ASME J. Engng Gas Turbines Power* **106,** 252–257 (1984).
20. W. M. Kays and M. E. Crawford, *Convective Heat and Mass Transfer* (2nd Edn), p. 199. McGraw-Hill, New York (1980).
21. D. E. Metzger, Z. X. Fan and W. B. Shepard, Pressure loss and heat transfer through multiple rows of short pin fins, *Proc. 7th Int. Heat Transfer Conf.*, Vol. 3, pp. 137–142 (1983).

APPENDIX. COMPARISON OF THE MASS TRANSFER RESULTS

1. Array-averaged Sherwood number reduced from equation (14):

$$\text{UDCF:}\quad \overline{Sh}_d = 0.299\,Re_{d,max}^{0.653} = 0.417\,Re_{d,ave}^{0.653}$$

$$\text{SDCF1:}\quad \overline{Sh}_d = 0.326\,Re_{d,max}^{0.653} = 0.437\,Re_{d,ave}^{0.653}$$

$$\text{SDCF2:}\quad \overline{Sh}_d = 0.330\,Re_{d,max}^{0.653} = 0.433\,Re_{d,ave}^{0.653}.$$

2. Fully developed Sherwood number reduced from equation (15):

$$\text{UDCF:}\quad Sh_{d,f} = 0.327\,Re_{d,max}^{0.647} = 0.455\,Re_{d,ave}^{0.647}$$

$$\text{SDCF1:}\quad Sh_{d,f} = 0.360\,Re_{d,max}^{0.647} = 0.481\,Re_{d,ave}^{0.647}$$

$$\text{SDCF2:}\quad Sh_{d,f} = 0.367\,Re_{d,max}^{0.647} = 0.481\,Re_{d,ave}^{0.647}.$$

3. Relative mass transfer performance evaluated using the above equations:

Flow condition	Ratio	$\frac{(\overline{Sh}_d)_{SDCF}}{(\overline{Sh}_d)_{UDCF}}$	$\frac{(\overline{Sh}_d A_w)_{SDCF}}{(\overline{Sh}_d A_w)_{UDCF}}$	$\frac{(Sh_{d,f})_{SDCF}}{(Sh_{d,f})_{UDCF}}$	$\frac{(Sh_{d,f} A_w)_{SDCF}}{(Sh_{d,f} A_w)_{UDCF}}$
Same $Re_{d,max}$	SDCF1/UDCF	1.0954	1.1254	1.1017	1.1319
	SDCF2/UDCF	1.1045	1.0788	1.1235	1.0974
Same $Re_{d,ave}$	SDCF1/UDCF	1.0462	1.0749	1.0573	1.0863
	SDCF2/UDCF	1.0383	1.0142	1.0567	1.0322

The parameters used in these calculations are

$$\left(\frac{Re_{d,ave}}{Re_{d,max}}\right)_{UDCF} = 0.60,\quad \left(\frac{Re_{d,ave}}{Re_{d,max}}\right)_{SDCF1} = 0.6394,\quad \left(\frac{Re_{d,ave}}{Re_{d,max}}\right)_{SDCF2} = 0.6596,\quad \frac{(A_w)_{SDCF1}}{(A_w)_{UDCF}} = 1.0274,\quad \frac{(A_w)_{SDCF2}}{(A_w)_{UDCF}} = 0.9768.$$